RSC Advances

ROYAL SOCIETY OF CHEMISTRY

www.rsc.org/advances

Graphical abstract

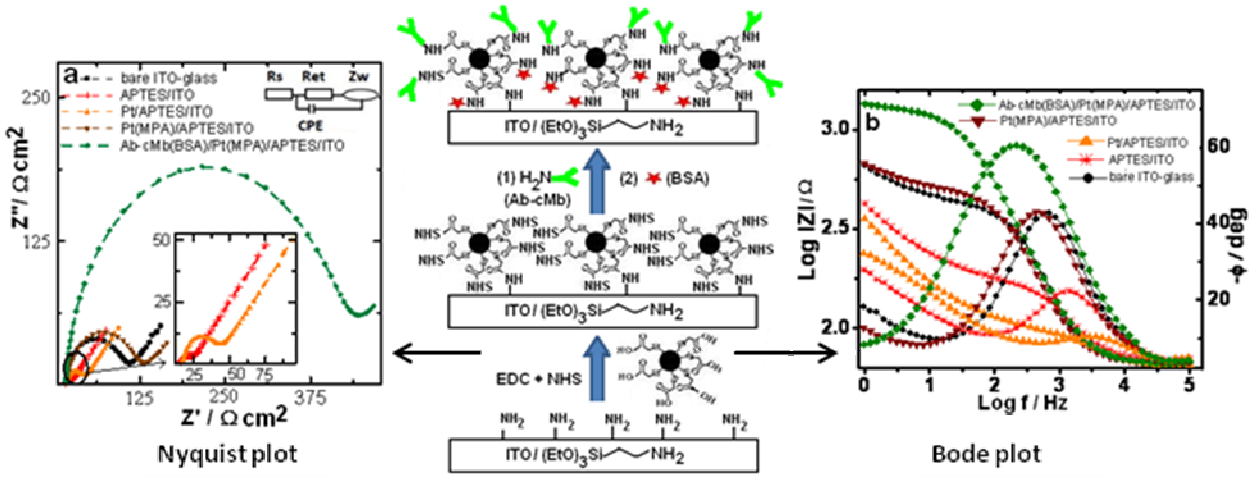

Cite this: DOI: 10.1039/c0xx00000x

www.rsc.org/xxxxxx

ARTICLE TYPE

Bio-functionalized Pt nanoparticles based electrochemical impedance immunosensor for human cardiac myoglobin

Sujeet K Mishra [a,b], Avanish K Srivastava [a], Devendra Kumar [b] and Rajesh [a*]

Received (in XXX, XXX) Xth XXXXXXXXX 20XX, Accepted Xth XXXXXXXXX 20XX

DOI: 10.1039/b000000x

Abstract

We report covalent immobilization of 3-Dimensional carboxyl functionalized Pt(MPA) nanoparticles with myoglobin protein antibody by carbodiimide coupling reaction deposited onto an indium-tin-oxide coated glass plate for the construction of a bioelectrode. This bioelectrode assembly was characterized by spectro/microscopic and electrochemical techniques. The Electrochemical impedance studies of the bioelectrode showed significant changes in charge transfer resistance (R_{et}), predominantly at low ac frequency region of < 40 Hz on immunoreaction with human cardiac myoglobin antigen (Ag-cMb) and exhibited a linear range of 0.01 μg mL^{-1} to 1 μg mL^{-1} Ag-cMb detection in phosphate buffer with a sensitivity of 184.8 Ω cm^2 per decade

1. Introduction

Nanostructured materials such as nanoparticles, nanotubes, and nano hybrid materials have aroused dramatic interests and have become an intensive research area due to their unique chemical and physical properties, such as large specific surface areas, good biocompatibilities, and high surface free energies.[1] The recent advances in the field of nanotechnology have opened up research opportunities on materials with ultrafine nanostructures. Metal nanoparticles with their fascinating properties such as large surface-to-volume ratio and the increased surface activity, have continued to draw a great deal of attention by interdisciplinary areas of the scientific community and incur intriguing applications in many fields of physical, chemical and material sciences in the past few years.[2–4] Recently, the amount of research on their biological applications has increased with potential applications in the construction of electrochemical sensors and biosensors, where they function as "electron antennae" efficiently channeling electrons between the electrode and the electroactive species. [5-6] Functionalized nanomaterials have offered excellent prospects for interfacing biological recognition events with electronic signal transduction leading to the design of a new generation of bioelectronic devices that exhibit novel functions. The major advantage of using functionalized nanomaterials is their potential capacity for combining multiple modalities within a single probe which enables far higher sensitivities to be achieved. Platinum (Pt), one of the most researched noble metals, has extensive application in the field of electrochemical sensors as they can act as an effective matrix of biomolecules by taking advantage of their biocompatibility and huge surfaces of Pt nanoparticles. [7] Recent applications of Pt nanoparticles include the detection of low concentrations of DNA by employing a platinum nanoparticle–gold ultra microelectrode in a hydrazine oxidation reaction. [8]

According to WHO report (2011), cardiovascular diseases (CVD) are considered to be the leading cause of death around the world. [9] CVD include coronary heart disease, cerebrovascular disease, raised blood pressure, peripheral artery disease, rheumatic heart disease and congenital heart disease and heart failure. Cardiac markers are biological analytes that are detectable in the blood serum and plays an essential role in the diagnosis, prognosis, monitoring, and risk stratification of suspected CVD patients. [10] Among currently used cardiac markers for the detection of acute myocardial infarction (AMI) [11], Myoglobin (found in heart and skeletal muscles) whose concentration in blood rises quickly, i.e. 1–3 h after the appearance of initial symptoms of the disease, and reaches the maximum between 6 and 12 h while returning to the baseline within 24–48 h, has been proven to be a valuable screening test for its early diagnosis. Myoglobin (cMb), a 17.6 kDa monomeric hemeprotein, has 153 amino acid residues in a highly folded and compact structure with eight separate and distinct alpha helical secondary structures. Due to its small size with molecular dimension of 3 nm×4 nm×5 nm and molar volume of 1.87 × 10^4 cm^3 mol^{-1} [12], it is quickly released into circulation which makes cMb a valuable early screening test for AMI. The normal cMb level found in human blood ranges from 30 to 90 ng mL^{-1} which shoots up to 200 ng mL^{-1} or even higher within 1 h of onset of myocardial infarction and can go up to as high as 900 ng mL^{-1} during the peak hour. In general, tests for detecting cMb are either indicative rapid tests, or they are estimated using sandwich immunoassay with secondary labeled antibodies, i.e. enzyme linked immunosorbent assay (ELISA) technique. However, they require laboratory equipments with proper instrument, multi-step processing of samples, and well-trained personnel, leading to considerable time consuming and expense to the overall detection. Masson et al developed a surface plasmon resonance (SPR) based sensor for

Myoglobin.[13] This type of detection using SPR phenomenon is relatively easy and cheap to perform that also allows quantitative/kinetic measurement of molecular interactions but the main problem associated with SPR sensor is fouling ability, low affinity and specificity that affect sensitivity of biosensing transducers. Other type of optical biosensors used for Mb detection includes, such as developed by Darain et al [14] and Matveeva et al [15] that can perform enhanced Mb immunoassays but these are expensive and require dedicated personnel to perform the tests. Also, they require difficult labeling procedures that depend on indirect indicator based signal schemes. Matveeva et al have utilized silver island films (SIF) for developing a fluorescence based immunoassay for the cardiac Mb. However, the main disadvantageous of this method is the non-homogeneous nature of SIFs, which results in significant deviations in assay readings and is therefore not suitable for the precise Mb detection. [15]

Electrochemical immunosensors are an important class of sensing systems which has revolutionized the modern chemical analysis because of their easy use, high efficiency, possibility of portability and miniaturization, fast response time and a direct transduction of the bio-molecular recognition event into electronic signals. Due to high accuracy, sensitivity, selectivity and cost-effectiveness they have been extensively used to detect proteins, biomarkers, biological toxins and biological-warfare agents in critical situations, food, environment, pharmaceutical chemistry, and clinical diagnostics.[16-20] Pakapongpan et al. [21] have reported an electrochemical sensor for Mb based on methylene blue-multiwalled carbon nanotubes (MWCNT) nanohybrid modified glassy carbon electrode (GCE), which is based on a direct electrochemical reduction of Mb. Though, the sensor provided a wide linear range of Mb detection from 0.1 µM to 3.0 µM (~1.78 µg mL^{-1} to 53.40 µg mL^{-1}), it is out of physiological range of cMb in human blood and thus would require a sample dilution for low level sub µg mL^{-1} Mb detection.

Electrochemical impedance spectroscopy (EIS) has recently received considerable attention for providing a sensitive and non-destructive characterization of the electrical properties in biological interfaces such as sensing formation of antigen–antibody and biotin–avidin complexes and interactions between oligonucleotides and DNAs [22-23].

In this paper, considering the advantages of EIS method and the properties of metal Pt nanoparticles, we report a platform for the construction of a bioelectrode for the detection of cardiac biomarker, cMb, using functionalized Pt nanoparticles. The functionalized Pt nanoparticles are covalently anchored on the self assembled monolayer (SAM) of 3-aminopropyltriethoxy silane (APTES) over an indium-tin-oxide (ITO)-glass plate. Subsequently, the cardiac protein antibody, Ab-cMb, is covalently attached to the carboxyl functionalized Pt nanoparticle-modified APTES/ITO-glass plates using carbodiimide coupling reaction. This bioelectrode is systematically characterized by various microscopic techniques and its immunosensing characteristic towards the quantitative estimation of the cardiac biomarker antigen, Ag-cMb, in phosphate buffer saline (PBS; pH7.4) is investigated by EIS technique using $[Fe(CN)_6]^{3-/4-}$ as a redox probe.

2. Experimental

2.1 Reagents

Monoclonal mouse anti-human cardiac myoglobin (Ab-cMb; Cat 4M23) and Myoglobin derived from human heart tissue (Ag-cMb; Cat 8M50) were procured from Hytest (Turku, Finland). Mouse immunoglobulin-G (Ag-IgG) (Cat IGP3) is obtained from GENEI, Bangalore, India. 3-Aminopropyl triethoxysilane (APTES) was purchased from Merck chemicals (Germany). N-(3-dimethyl aminopropyl)-N'-ethyl carbodiimide hydro chloride (EDC) and N-hydroxy succinimide 98% (NHS), Hydrogen hexachloroplatinate hexahydrate ($H_2PtCl_6 \cdot 6H_2O$), Sodium borohydride ($NaBH_4$) and 3-mercaptopropionic acid (MPA) were obtained from Sigma-Aldrich Corp. All other chemicals were of analytical grade and used without further purification.

2.2 Apparatus

Contact angles were recorded on Drop Shape Analysis System; model DSA10MK2 from Krüss GmbH, Germany. XRD pattern were recorded using Bruker AXS Advance D8 powder X-ray diffractometer. High resolution transmission electron microscopy was performed on HRTEM model: Tecnai G2 F30 STWIN with field emission gun, operated at 300 kV. Scanning electron microscopy (SEM) images were obtained with a LEO 440 PC; UK based digital scanning electron micrograph with a mounted energy dispersive X-ray spectrometer (EDX). A Fourier-transform infrared (FTIR) spectrum was taken on Perkin- Elmer, Spectrum BX II. Atomic force microscopy (AFM) images were obtained on a Nanoscope 5, VEECO Instrument Ltd., USA. Cyclic voltammetry and EIS measurements have been done on a PGSTAT302N, AUTOLAB instrument from Eco Chemie, The Netherlands.The EIS experimental data were circuit fitted by GPES (General purpose electrochemical system version 4.9, Eco Chemie) software and values of EIS parameters were obtained.

2.3. Synthesis of functionalized Pt nanoparticles

3-mercaptopropionic acid capped Pt (MPA) nanoparticles were chemically synthesized using conventional sodium borohydride reduction method in aqueous solution as reported earlier, with slight modification. [24] Briefly, a 100 mM stock solution of Pt salt was prepared by dissolving 1 g of $H_2PtCl_6 \cdot 6H_2O$ in 19 mL deionized water. 1 mL of this stock solution was then subsequently reduced by adding drop wise $NaBH_4$ solution (48 mg in 2 mL H_2O) under constant stirring. The change in color of the solution from yellow to dark brown indicated the formation of the Pt nanoparticles. A solution of 46µL MPA in 10 mL H_2O was then immediately added to stabilize the above Pt colloidal solution and the final volume of the reaction mixture was kept at 50 mL. The reaction mixture was left for stirring for 2 h at room temperature. Thereafter, the colloidal solution was washed 2 to 3 times with ethanol and centrifuged at 20000 rpm, and vacuum dried for 12 h.

2.4. Preparation of bioelectrode

The ITO coated glass plates (10Ω /□) were cleaned by sequential ultrasonic cleaning in extran, acetone, ethanol, isopropyl alcohol and DI for 10 min each and dried in vacuum. The cleaned ITO glass plates were then exposed to oxygen plasma for 5 minutes in a plasma chamber to increase the amount of hydroxyl groups

present on the ITO-glass surface. After this, these ITO glass plates were immersed in 2% APTES solution prepared in ethanol for 1.5 h, under the ambient conditions, to form a SAM of APTES and then subsequently rinsed with ethanol in order to remove non-bonded APTES from the surface of the substrate and dried under N_2 gas flow. The carboxyl groups present on the Pt(MPA) nanoparticles were first activated to prepare amine-reactive esters of carboxylate groups by adding 30 mM NHS and 150 mM EDC in 5 mL aqueous solution of 0.1 mg mL^{-1} Pt(MPA) nanoparticles. The APTES modified ITO glass plates were then immersed in the above solution mixture of activated functionalized Pt(MPA) nanoparticles for 3 h, followed by washing with double distilled water and dried under N_2 gas flow to obtain Pt (MPA-NHS)/ APTES/ITO-glass. The cardiac myoglobin protein antibody (Ab-cMb) was immobilized onto the above said modified electrode by treating it with a phosphate buffer solution (PBS, pH 7.4) containing 100 µg mL^{-1} Ab-cMb, for overnight period at 4 °C, followed by washing with PBS and drying under N_2 flow. The Ab-cMb immobilized electrode was then incubated in 1% BSA solution, for 30 min to block the nonspecific binding sites on the electrode surface, followed by washing with PBS to remove any physically adsorbed antibodies and dried under N_2 flow. The schematic representation of the stepwise fabrication of the prototype assembly of Ab-cMb/Pt(MPA)/APTES/ITO-glass electrode is shown in scheme1.

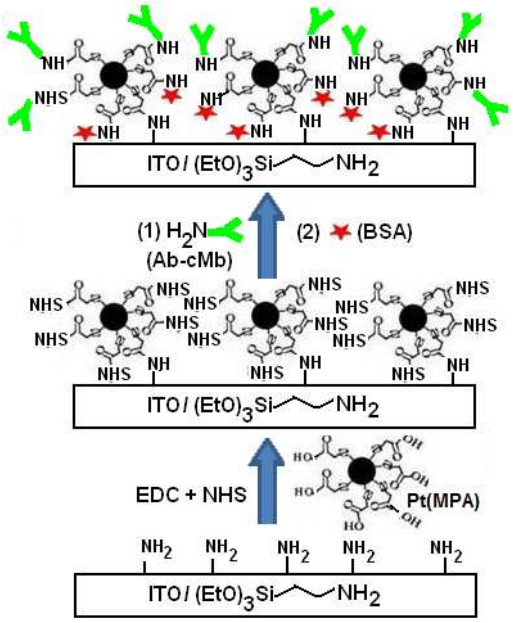

Scheme 1: Schematic representation of stepwise fabrication of the bioelectrode

2.5. EIS measurement procedure

All electrochemical measurements were carried out in a conventional three-electrode cell configuration consisting of the proposed modified electrode as working electrode, Ag/AgCl as a reference electrode and a platinum wire as a counter electrode. The electrochemical impedance spectroscopy has been conducted in PBS (pH 7.4, 0.1M KCl) solution containing 2 mM $[Fe(CN)_6]^{3-}$ /$[Fe(CN)_6]^{4-}$ in the frequency range from 1Hz to 100 KHz at an AC voltage of 0.05 V. From a stock solution of 100 µgmL^{-1} of protein antigen, Ag-cMb, aliquots of different concentrations were prepared in PBS. EIS response of the Ab-cMb/Pt(MPA)/APTES/ITO-glass bioelectrode was measured after the addition of successive aliquots of different concentrations of protein antigen Ag-cMb in PBS solution containing 2 mM $[Fe(CN)_6]^{3-}$/$[Fe(CN)_6]^{4-}$. An impedance measurement was conducted with a sample solution containing no Ag-cMb and the corresponding electron transfer resistance (R_{et}) observed in a Nyquist plot was taken as a control sample response. Subsequently, R_{et} with other related EIS parameters were measured after the successive addition of the aliquots of different concentrations of Ag-cMb solution for the detection of antibody–antigen immunoreaction.

3. Results and discussion

3.1. Contact angle measurement

Contact angle measurement based on the sessile drop method was used to determine the hydrophobic/ hydrophilic character of the electrode surface using water droplets as the test liquid probe. It offers an easy-to-measure indication of the nature of the functional groups present on the uppermost surface layers of the modified electrode surface. Water droplets were manually introduced onto the electrode surface with a micro syringe and the digital snapshots were taken of the droplets on the surface and analyzed with software provided by Kruss. Four replicates for each measurement at different steps of modifications were taken to establish statistical significance. The bare ITO-glass electrode with its surface hydroxyl groups shows hydrophilic behavior with a contact angle (θ) value of 40 ±1° (fig 1a). The surface polarity alters after the modification of the ITO-glass electrode by hydrophobic alkyl chains of APTES molecules that decrease the surface energy by drastically reducing the hydroxyl groups of the bare ITO-glass on silanization and increases the value of θ to 78 ±1° (fig 1b). The covalent attachment of Pt(MPA) nanoparticles on APTES/ITO-glass leads to the formation of a hydrophilic surface comprising of carboxyl groups which decreases the value of θ to 59 ± 2° (fig 1c). Further, after immobilization of the protein antibody the value of θ increases significantly to 91 ±1° (fig 1d) due to the substitution of hydrophilic carboxyl groups by hydrophobic amino acid chains of protein antibody molecules, thereby indicating the attachment of Ab-cMb molecules over the Pt(MPA) modified electrode surface assembly.

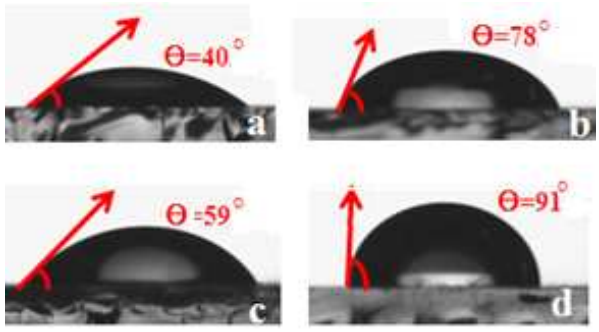

Fig.1. Contact angle measurement images of (a) ITO coated glass plate; (b) APTES/ITO-glass; (c) Pt(MPA)/APTES/ITO-glass; and (d) Ab-cMb/ Pt(MPA) /APTES/ITO-glass

3.2 Microstructural characteristics

XRD has been used to examine the possible crystallinity of the Pt nanoparticles formed after sodium borohydride reduction. Fig. 2 shows the X-ray diffraction pattern of the functionalized Pt nanoparticles. The sample exhibits broad characteristic diffraction peaks of Pt with face center-cubic (f.c.c.) structure (JCPDS, card No. 4-802). The strongest diffraction peak were located at 2θ of 39.46° (111) with other two strong peaks at 45.88° (200) and 67.32° (220), respectively. The existence of broad intense peaks in the X-ray spectra indicates the presence of Pt nanoparticles with the nanocrystal dimensions. Since the breadth remains almost consistent for each peak, then certainly, the broadening is due to crystallite size. By using XRD peaks, the average size of Pt nanoparticles can be estimated by the width of the reflection according to the Debye–Scherrer equation (Eqn. 1):

$$D = 0.9\lambda/\beta \cos\theta \quad (1)$$

The average particle size of the Pt nanoparticles was calculated to be about 5.14 nm.

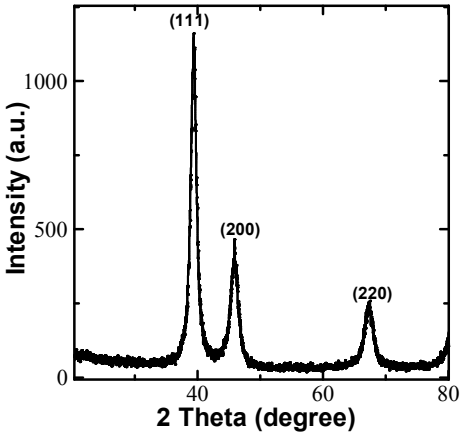

Fig.2. XRD Pattern of Pt nanoparticles

This was further confirmed by employing high resolution transmission electron microscopy. In general the microstructure was uniform with individual particles revealing facetted growth having sharp edges with a nature of intermingling to each other (Fig. 3a). At atomic scale it is obvious to see that there is good interfacing between the particles. Four numbers of such nanoparticles are clearly marked as A to D in Fig. 3b. Since most of the instances, these particles are overlapped and abutting to each other, a set of moiré fringes are also discerned (region marked as dotted circle in Fig. 3b). It is important to mention that at atomic scale the individual particles are interpreted as nano-crystallites with stacking of atomic planes in particular crystallographic orientations. The interplanar spacings of three such planes as 0.23, 0.20 and 0.14 nm corresponding to hkl: 111, 200 and 220, respectively, of Pt-face centered cubic structure (space group: $Fm\bar{3}m$, and lattice parameter: a = 0.39 nm, ref. JCPDS card no. 040802) are marked on the micrograph (Fig. 3b). The measurements carried out on Fig. 3a and b, further delineated that the size of these nanoparticles is on average between 4 to 5 nm (Fig. 3c), however in general these particles ranged between 1.5 to 8.5 nm on Gaussian graph.

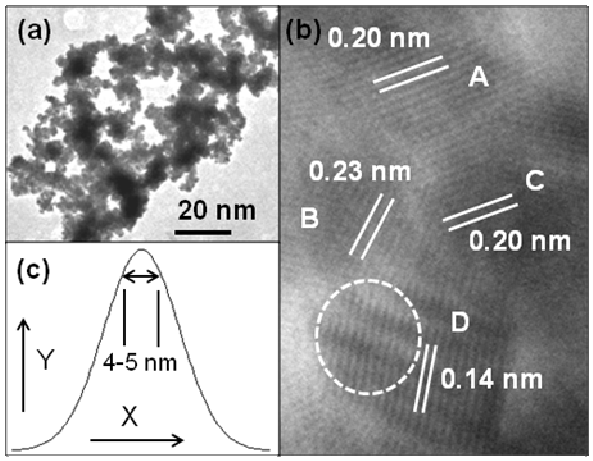

Fig.3. HRTEM micrographs showing (a) distribution of nanoparticles and (b) atomic scale images of different particles. (c) Gaussian size-distribution curve of the nanoparticles obtained from figs. (a) and (b). X-axis: 1.5 to 8.5 nm (size of particles) and Y-axis: 0 to 20 (no. of particles).

Figure 4 shows the typical EDX pattern of Pt-NPs functionalized APTES modified ITO-glass with an inset showing the SEM image of the corresponding electrode area. The EDX spectra demonstrate the presence of Pt-NPs along with other elements of the corresponding silane and ITO-glass. The SEM image shown in the Fig. 4 is one of the electrodes among the batch of 3 electrodes prepared simultaneously. SEM image shows metallic granular particles of Pt nanoparticles distributed over the modified electrode surface area.

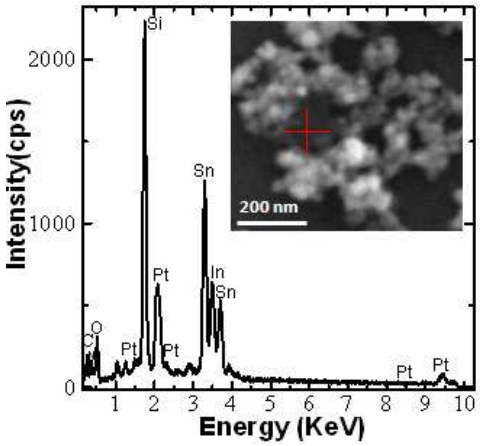

Fig.4. EDX spectra of Pt(MPA) nanoparticles on ITO and inset shows corresponding SEM area at the magnification of 50 KX.

Figure 5 shows FTIR spectra of the (a) APTES/ITO (b) Pt (MPA)/APTES/ITO and (c) Ab-cMb/Pt(MPA)/APTES/ITO taken on attenuated total reflection mode. For APTES (Fig. 5a) the spectrum shows the Si-O-Si characteristic band at 1055 cm^{-1} [25]. The characteristic peak observed at 1750 cm^{-1} (Fig. 5b) is due to the C=O stretching vibrations and of the carboxylic groups of the MPA functionalized Pt nanoparticles. Further the peaks at 2965 cm^{-1} and 936 cm^{-1} refers to the –OH stretching and bending vibrations of the carboxylic acid group. After the immobilization of protein antibody Ab-cMb, additional peaks at 3387 cm^{-1} and 1612 cm^{-1} (Fig. 5c), representing the N-H stretching and bending

vibrations [26] respectively was observed, which is indicative of the formation of amide bond by the Pt(MPA) nanoparticles with Ab-cMb molecules.

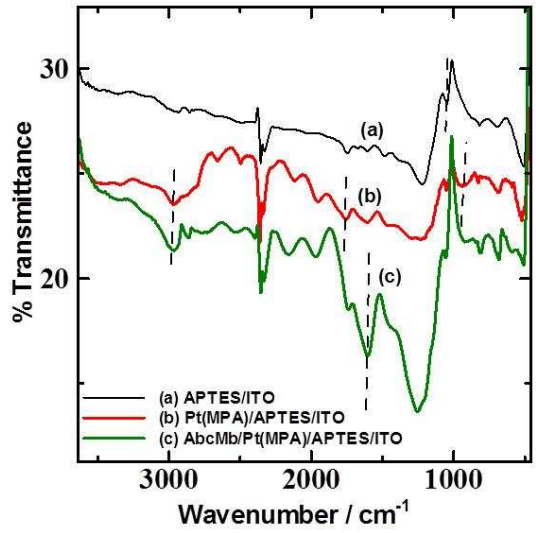

Fig.5. FTIR spectra of (a) APTES/ITO-glass (b) Pt(MPA)/ APTES/ITO-glass and (c) Ab-cMb/Pt(MPA)/APTES/ITO-glass

The surface morphology of the each modified step involved in the fabrication of Pt(MPA) modified bioelectrode was characterized by using atomic force microscopy (AFM) images taken in a non contact mode (Fig. 6).

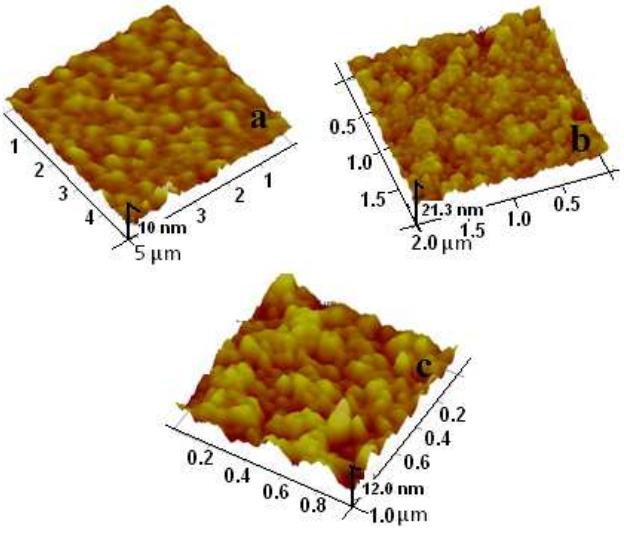

Fig.6. AFM images of (a) APTES/ITO-glass (b) Pt(MPA)/ APTES/ITO-glass and (c) Ab-cMb/Pt(MPA)/APTES/ITO-glass

The surface roughness parameter (R_a) and root mean square roughness (R_q) are the two amplitude parameters that has been used to study the temporal changes occurred in the creation of a new surface, and spatial differences when studying the surface feature using different scales in terms of irregularity and height distribution. Fig. 6a shows the AFM image of the SAM of APTES on ITO-glass surface having a regular island-like structure with only a few surface aggregates. The corresponding R_a and R_q of APTES/ITO-glass surface are 0.886 nm and 1.08 nm respectively. The surface morphology changes to a dense and complete one with granular particles spreading all over it on modification with Pt(MPA) nanoparticles (Fig. 6b) ,showing an increased values of both R_a and R_q to 1.56 nm and 1.95 nm, respectively. However, the AFM image (Fig. 6c) of the bioelectrode shows a completely changed morphology upon protein Ab-cMb immobilization with an appreciable increase in R_a value of 1.72 nm and R_q of 2.12 nm, exhibiting a comparatively much bigger and more globular feature characteristic to protein nature. [27] This significant increase in both the R_a and R_q values indicated the immobilization of the Ab-cMb molecules well over the surface of Pt-NPs modified electrode.

3.3 Electrochemical characterization of the bioelectrode

EIS has been chosen as the main characterization technique to assess the immunosensor performance, since it is known as an effective tool for the qualitative and quantitative characterization of electrochemical processes occurring at the electrode/solution interface of the modified electrode. EIS monitors response of the studied system to the application of a small amplitude AC signal at different frequencies. Although this technique does not lead to the identification of the chemical bonds or of the intermediates but vital information regarding the reaction rates occurring at the electrode/solution interface can be obtained. This is usually done using an 'equivalent circuit' which comprises of an assembly of electrical circuit elements that model the physicoelectric characteristics of the electrode/solution interface. In the present work the experimental fitted Randle's equivalent circuit model was employed which includes the following four elements: (i) the ohmic resistance of the electrolyte solution, R_s; (ii) the Warburg impedance, Z_w, resulting from the diffusion of ions from the bulk electrolyte to the electrode interface; (iii) the interfacial double layer capacitance (C_{dl}) between an electrode and a solution, relating to the surface condition of the electrode and (iv) the electron-transfer resistance, R_{et}. This equivalent circuit model has been modified by a constant phase element (CPE) instead of the classical capacitance to incorporate the Helmholtz double layer and surface roughness or heterogeneity of the electrode and is in a parallel arrangement with both R_{et} and Z_w, all of which are in a series arrangement with R_s. The impedance related to CPE is given by eqn.2:

$$Z_{CPE}(\omega) = 1/Z_0 (j\omega)^n \quad (2)$$

where Z_0 is a constant, j is the imaginary number, ω the angular frequency, and n is the CPE exponent which can be used as a gauge of the heterogeneity and gives details about the degree of surface inhomogeneity (roughness). Depending on the value of n, CPE can represent resistance (n = 0, Z_0 = R), capacitance (n= 1, Z_0=1/*C*), inductance (n = -1, Z_0 = *L*) or Warburg element (n = 0.5). As shown in Table 1, the values of exponent n are close to 1, indicating there minimal defects in the modification layer on the electrode surface and also CPE, in our case resembles a pseudo capacitor. Nyquist plots (real part of the impedance Z' vs. imaginary part -Z″) has been used to represent the impedance behavior of the different modified electrodes. These plots

Cite this: DOI: 10.1039/c0xx00000x

www.rsc.org/xxxxxx

ARTICLE TYPE

Table 1.EIS characteristic parameters at various stages of surface modification of the electrodes

Type of Electrodes	R_{et} (Ωcm^2)	CPE Z_0 (μFcm^{-2})	CPE n	Z_w ($x10^{-3}$) (Ωcm^2)	χ^2 ($x10^{-4}$)	δ (μm)
ITO-glass	85.7	2.76	0.93	3.45	1.88	55.44
APTES/ ITO	25.2	4.82	0.87	3.42	1.13	49.69
Pt(MPA)/ APTES/ ITO	107.0	3.07	0.88	3.67	1.99	61.68
Pt/ APTES/ ITO	9.0	13.19	0.77	3.22	1.38	47.09
Ab-cMb/Pt(MPA)/ APTES/ ITO	183.5	2.44	0.96	3.90	2.30	72.74

R_{et}=charge transfer resistance; CPE=constant phase element; δ=diffusion layer thickness; Z_w = warburg resistance

typically exhibit two important regions: (i) a semicircle at high frequencies, describing the Faradaic electron transfer process (in which the semicircle diameter equals the R_{et}); (ii) a straight region at lower frequencies, depicting the diffusion-limited transport of the redox species from the electrolyte to the electrode interface. Small value of χ^2 (Chi-square) of the order of 10^{-4} so obtained suggest that the selected fitting circuit model could give appropriate results (table1). Figure 7a shows the Nyquist plot of different modified electrodes with equivalent circuit shown in inset. The bare ITO-glass shows a R_{et} value of 85.75 Ω cm^2 (table 1) which sharply reduces to 25.22 Ω cm^2 for the APTES/ITO-glass indicating an easy electronic transport at the electrode surface interface. This reduction in the R_{et} value with a comparatively high Z_0 value of 4.82 μF cm^{-2} is attributed to an increased concentration of the anionic probe $[Fe(CN)_6]^{3-/4-}$ at the electrode/solution interface due to its strong affinity towards the polycatonic layer, as the amino groups of the APTES get protonated (NH_3^+) in aqueous solution. After the covalent attachment of the Pt(MPA) NPs to silane layer the R_{et} value increases sharply to 107.0 Ω cm^2 and Z_0 decreases to 3.07 μFcm^{-2} due to the charge repulsive behavior of the negatively charged carboxyl groups of Pt(MPA) NPs at pH 7.4 towards the anionic probe at the electrode/solution interface. To further establish the presence of carboxyl groups at the modified electrode surface, EIS study was performed on non-carboxyl functionalized Pt NPs (without MPA capping) modified APTES/ITO-glass electrode. As can be seen from the corresponding Nyquist plot obtained, the decreased diameter of the semicircle with a sharp decrease in the corresponding R_{et} value to 9.0 Ω cm^2 indicates the unconstrained transfer of electrons from the probe towards the electrode surface. This extremely high relative signal change Δ R_{et} (~1088 %) that has been observed at Pt(MPA)-NPs modified electrode with respect to Pt-NPs modified electrode constitutes great evidence for the high population of free carboxyl groups on the surface of Pt(MPA)/APTES/ITO-glass electrode. Further, covalent immobilization of cardiac myoglobin protein antibody on Pt(MPA)-NPs over the electrode surface and subsequent blocking of the non-specific binding sites by BSA significantly increases the R_{et} value to 183.5 Ω cm^2 and reduces the Z_0 to 2.44 μF cm^{-2} reflecting the insulating behavior of the protein molecule which inhibits both charge and mass transfer of the probe towards the electrode surface.

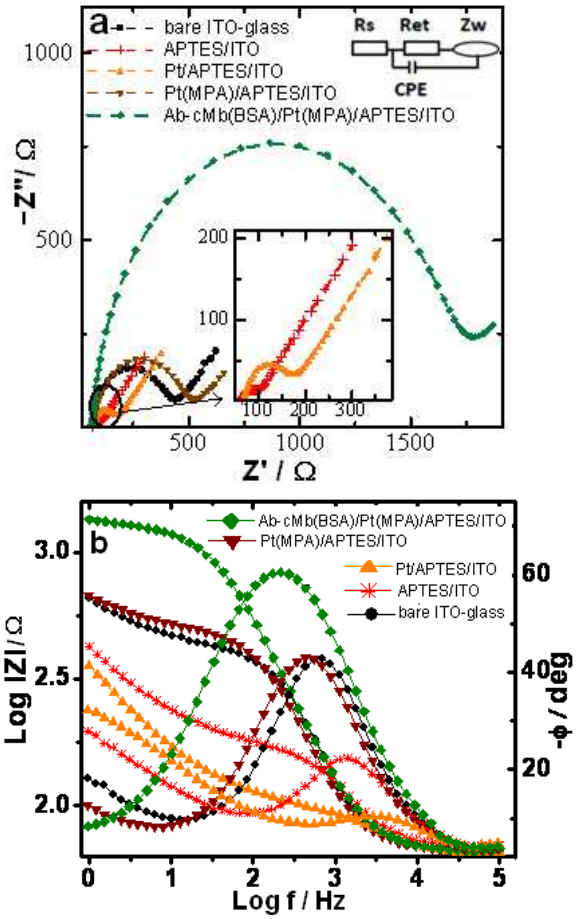

Fig.7. (a) Nyquist plots obtained for bare ITO glass plate; APTES/ITO-glass; Pt(MPA) / APTES /ITO-glass; Pt / APTES /ITO-glass and Ab-cMb(BSA)/ Pt(MPA) /APTES/ITO-glass in PBS (pH 7.4,0.1M KCl) containing 2mM $[Fe(CN)_6]^{3-/4-}$; (b) Corresponding bode plots

A more clear description of the frequency-dependent behavior of different circuit elements of the fitted Randles' circuit is provided by the Bode plots as shown in Fig. 7b. Valuable information regarding certain kinetic phenomena occurring at the electrode/solution interface at different ranges of frequencies applied can be obtained from these plots. It is noticeable from the

plot that at very low frequency region of <10 Hz, a diffusive nature is obtained for APTES/ITO-glass electrode which on modification by Pt(MPA) nanoparticles is somewhat reduced and which finally disappears on immobilization of protein Ab-cMb on the modified electrode. The dominance of R_{et} behavior in the low frequency region for the bioelectrode reflects the presence of biocompatible nature even at such low frequency.

Davies and Compton proposed a term known as the diffusion layer thickness δ, which helps in categorizing the type of diffusion occurring at the modified electrodes. The value of δ can be obtained from the modified Einstein equation for the root mean square displacement of diffusing particles [28] as shown in eqn. 3 and listed in table 1:

$$\delta = (2D\Delta E/\upsilon)^{1/2} \quad (3)$$

where D is diffusion coefficient of aqueous ferrocyanide (6.3 x 10^{-6} cm^2s^{-1}), ΔE is the potential width of the votammogram and υ is the scan rate (0.05 Vs^{-1}). The δ value obtained for the bioelectrode shows a case 3 type behavior of the voltammetric response that corresponds to a spatially heterogeneous electrode. This phenomenon is associated with an overlap of adjacent diffusion layers resulting from the small size of the inert part of the electrode. [28]

3.4 Surface coverage and nature of the bioelectrode

The value of the fractional coverage area (θ) of the functionalized Pt-NPs over the SAM of silane can be calculated from the impedance diagram using the eqn. 4 [29]:

$$\theta = 1 - R_{et1} / R_{et2} \quad (4)$$

where R_{et1} and R_{et2} represents the surface specific charge transfer resistances of SAM modified APTES/ITO-glass and Pt(MPA)-NPS modified APTES/ITO-glass, respectively. The value of θ was found to be 0.76, indicating a more than 76% surface coverage of the SAM modified electrode by Pt(MPA)-NPs.

The type of electrochemical mechanism occurring at the electrode/electrolyte interface of the Ab-cMb/Pt (MPA)/APTES/ITO-glass bioelectrode can be obtained from the relationship between the peak current and the scan rate. Figure 8 shows the Cyclic Voltammogram (CV) of the resulting bioelectrode in 2mM $[Fe(CN)_6]^{3-/4-}$ at different scan rate from 25-125 mVs^{-1} and a plot of the anodic (I_{pa}) and cathodic peak currents (I_{pc}) versus square root of the scan rates ($v^{1/2}$) (inset of Fig. 8).

A linear relationship with good correlation coefficients between the peak currents and the square root of scan rate was obtained suggesting a diffusion controlled process occurring at the bioelectrode/solution interface. The linear regression line so obtained between the anodic peak current I_{pa} and $v^{1/2}$ can be expressed by the eqn. (5),

$$I_{pa}(v^{1/2}) = b\, v^{1/2} + c \quad (5)$$

where slope b = 6.90 μA $(mV\ s^{-1})^{-1/2}$ and the intercept c is 22.4 μA, having a correlation coefficient of 0.996.

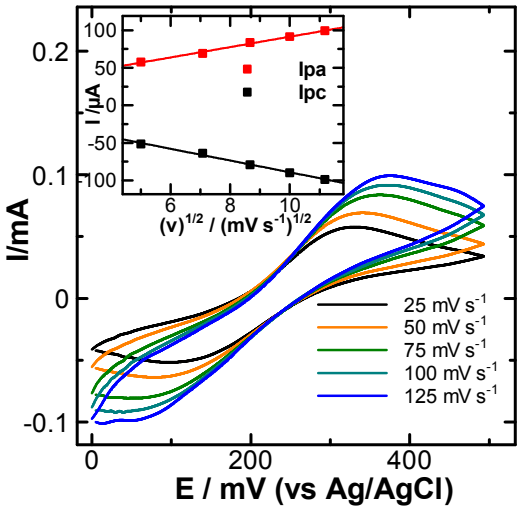

Fig.8. CV of bioelectrode as a function of scan rate in PBS (pH 7.4, 0.1M KCl) containing 2mM $[Fe(CN)_6]^{3-/4-}$. Inset: plot of peak current vs $v^{1/2}$ (mV/s).

3.5 Electrochemical impedance response of the bioelectrode towards protein antigen Ag-cMb

The specific immunoreaction of Ab-cMb to its complimentary target Ag-cMb at the electrode surface results in the formation of an antibody-antigen complex. The formation of immunocomplex results in the creation of a kinetic barrier which perturbs the interfacial electron transport, at the bioelectrode/solution interface. As the Faradaic reaction of a redox couple becomes increasingly hindered, the electron transfer resistance increases and the capacitance decreases accordingly. The sample solution without a target protein, Ag-cMb, has been taken as the control sample and the corresponding R_{et} value as the control sample response. Figure 9a shows the Nyquist plots obtained after the subsequent addition of successive aliquots of different concentration of target protein antigen and the corresponding fitting values of R_{et} are given in table 2. The plot shows noticeable increment in the diameter of the Nyquist circles with increasing concentration of the added protein antigen Ag-cMb based on antigen-antibody interaction. A small but noticeable decrease in Z_0 values was also observed with subsequent immunoreaction indicating a decrease in capacitive behavior of the bioelectrode with immunoreaction.

The corresponding Bode frequency spectrum upon the above immunoreactions occurring at the electrode surface is shown in fig 9b. In the high frequency region of f >4 kHz the total impedance log |Z| remains unchanged with a phase angle (φ) of ~0° indicative of unchanged electrolyte solution resistance, R_s. In the intermediate frequency range i.e. from 4 kHz to 40 Hz almost a straight line curve was obtained with φ value of > 55° but < 90° which is indicative of pseudo capacitance behavior of the bioelectrode in this frequency range. Negligible changes with the addition of target Ag-cMb in the sample solution were observed in this region, which indicated that the proposed bioelectrode cannot function as a capacitive immunosensor. At low frequency region (f<40 Hz), visible changes were observed in the impedance modulus lines upon immunoreactions with the increasing concentration of added target Ag-cMb. As this region is dominated by R_{et}, this has consolidated our choice of using

Cite this: DOI: 10.1039/c0xx00000x

www.rsc.org/xxxxxx

ARTICLE TYPE

Table 2. EIS characteristic parameters upon immunoreactions with different concentrations of protein, Ag-cMb

Concentration of Ag-cMb	R_{et} (Ωcm^2)	CPE (Z_0) (μFcm^{-2})	n	Z_w ($x10^{-3}$) (Ωcm^2)	χ^2 ($x10^{-4}$)
Control	183.5	2.44	0.960	3.90	2.30
0.01µg mL^{-1}	288.3	2.26	0.970	2.20	2.10
0.05µg mL^{-1}	406.5	2.18	0.974	1.37	2.01
0.10µg mL^{-1}	494.3	2.15	0.976	1.02	2.74
0.50µg mL^{-1}	601.5	2.13	0.974	0.92	2.67
1.00µg mL^{-1}	647.8	2.08	0.979	0.82	3.12

changes in R_{et} as the main sensing element.

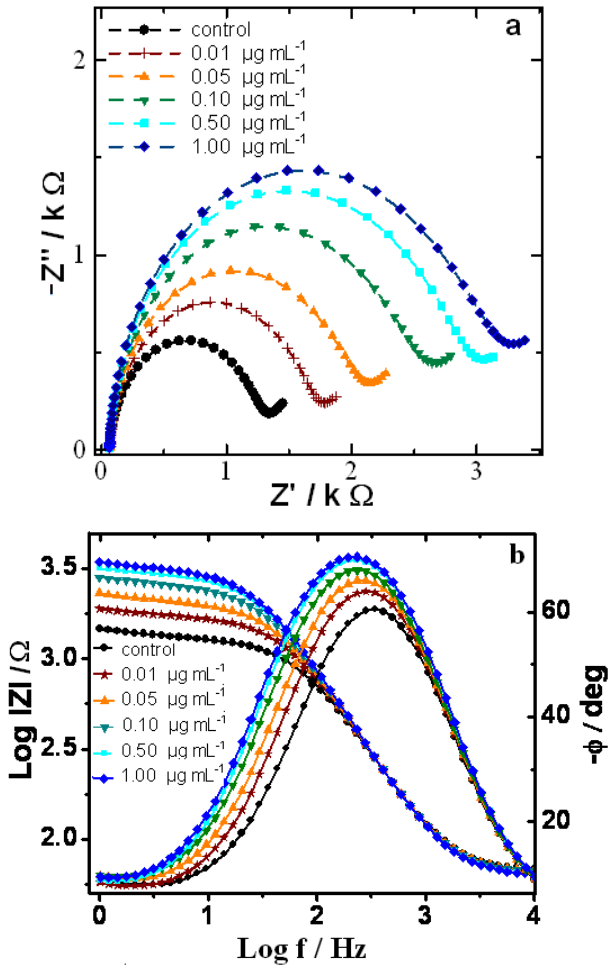

Fig.9.(a)Faradaic impedance spectra of the Ab-cMb(BSA)/Pt(MPA) /APTES/ITO-glass electrode before and after incubating with different concentration of Ag-cMb in PBS (pH7.4) with 0.1 M KCl solution containing 2 mM $[Fe(CN)_6]^{3-/4-}$, (b) Corresponding bode plots.

The sensitivity of the as prepared bioelectrode was obtained by plotting a graph (fig.10) between the change in specific electron charge transfer resistance ($\Delta R_{et} = (R_{et})_{after\ immunoreaction} - (R_{et})_{control}$) and logarithmic value of target Ag-cMb concentration in the range of 10 ng mL^{-1} to 1 µg mL^{-1}.

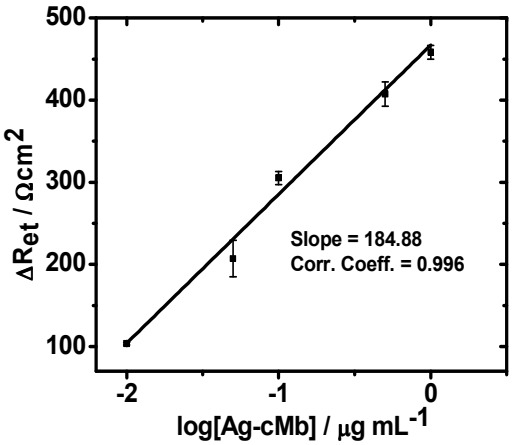

Fig.10. Concentration dependent calibration curve of bioelectrode; the error bars represent the standard deviation from three separate experiments.

Eqn. 7 depicts the linear relationship so obtained with slope of the line as the sensitivity of the bioelectrode:

$$\Delta R_{et}(\log [\text{Ag-cMb}]) = b \log [\text{Ag-cMb}] + d \qquad (7)$$

The R_{et} sensitivity (slope b of the calibration curve) of the bioelectrode was found to be 184.8 Ω cm^2 per decade of Ag-cMb with an intercept d = 473.74 Ω cm^2 having a correlation regression coefficient of 0.996 (n = 5). The limit of detection was found out to be 1.70 ng mL^{-1} based on three times of signal-to noise ratio.

This EIS experimental procedure requires about 12 minutes for complete assay including 3 minutes for the sample preparation without undergoing any pretreatment (compared to a few days for ELISA) showing its potential usefulness for the early detection of acute myocardial infarction (AMI). These results show that this bioelectrode is competitive with the other reported Mb sensors in terms of either physiological range of cMb detection with a minimum sample preparation time / experimental steps or high

Cite this: DOI: 10.1039/c0xx00000x

www.rsc.org/xxxxxx

ARTICLE TYPE

Table 3: Analytical performance of some electrochemical sensors for Mb detection

Electrochemical sensor type	Transduction platform	Linear range	Limit of Detection(LOD)	References
Flow injection analysis with amperometry	MB-MWNTs/GCE	1.78 μg mL^{-1} to 53.4 μg mL^{-1}	353.98 ng mL^{-1}	[21]
Impedimetric	SAM/Au electrode	10^{-12}–10^{-6} M	15 ng mL^{-1}	[35]
Potentiometric	SAM of alkane thiol/ gold-coated silicon chip	-	1000 ng mL^{-1}	[34]
Square wave voltammetry	SPE/MeNP-DDAB/anti-cMb	10 ng mL^{-1} to 400 ng mL^{-1}	5 ng mL^{-1}	[30]
cyclic voltammetry	TiO_2 nanotubes/ GCE	1 μg mL^{-1} to 100 μg mL^{-1}	1000 ng mL^{-1}	[33]
Impedimetric	MUA-MPA/Au-wire	10 ng mL^{-1} to 650 ng mL^{-1}	-	[32]
Impedimetric	Pt(MPA)/APTES/ITO	10 ng mL^{-1} to 1000 ng mL^{-1}	1.7 ng mL^{-1}	Present work

sensitivity than the recently reported semicondutor/metal nanoparticle/carbon nanomaterials and polymer based bioelectrodes.[15,21,30] A comparative analytical performance of some electrochemical based systems for Mb detection is given in Table 3. The high electroactive nature of the Pt(MPA) nanoparticles makes this bioelectrode more sensitive to Mb detection than the recently reported ZnS nanoparticles based bioelectrode which exhibited a comparatively low sensitivity of 117.36 Ω cm^2 per decade. [31]

The reproducibility of the bioelectrode was evaluated by measuring R_{et} response for each added concentration of the target Ag-cMb with three different bioelectrodes prepared independently, under similar experimental conditions. The inter-assay variation coefficient was found to be within the range of 1.5 to 18 % at individual Ag-cMb concentration, indicating an acceptable precision and fabrication reproducibility. The stability of the bioelectrode was examined by repeatedly carrying out the impedance measurements on the bioelectrode for the same sample of target Ag-cMb under identical conditions. It has been observed that even after 5 repeated impedance measurements, no appreciable changes in the impedimetric response was observed revealing the bioelectrode retains its biocompatible property both in the solution and in open as well. A sustained R_{et} response was obtained with individual bioelectrode, stored at 4°C, towards a fixed Ag-cMb concentration for at least two month, indicating a good shelf-life stability. The specificity of the bioelectrode towards the Ag-cMb was tested by carrying out the immunoreaction with non-specific mouse IgG, in the range of 10 ng mL^{-1} to 1 μg mL^{-1}, under identical conditions. No significant incremental changes were observed in the R_{et} values with the added aliquots of the IgG with respect to the control sample. This may be attributed to either the non-occurrence of antigen-antibody interaction or a weak non-specific interaction, if any, play insignificant role on evaluation of EIS spectra using this bioelectrode.

4. Conclusions

This work demonstrates a detail EIS characteristic of a bioelectrode based on functionalized Pt-NPs for the investigation of bioaffinity interaction towards the detection of prognostic cardiac marker, cMb. The functionalized Pt-NPs with large surface-to-volume ratio and free -COOH linkage groups remarkably improved the properties of the bioelectrode in terms of stability and sensitivity. Both the microstructural and electrochemical characteristics of the bioelectrode have been extensively characterized by AFM, TEM, XRD, EDX, and EIS techniques. The dominance of R_{et} behavior in the low frequency region of the EIS spectra of the bioelectrode exhibited the biocompatible nature. The bioelectrode shows a small capacitance change with high resistive component of impedance exhibiting the most specific and sensitive relationship to the electron transfer rate and hence thereby provided a direct response to antibody-antigen interaction on immunoreaction. High protein loading with efficient covalent bonding to the Pt-NPs results in the construction of a bioelectrode showing a wider linear detection range with good sensitivity, biocompatibility and acceptable reproducibility. Also, the protocol devised here is simple, efficient and inexpensive that can be used as a model for establishing general methods for the detection and quantitative analysis of other protein marker assays, after optimization with blood serum, in the field of clinical diagnostics and molecular biology.

Acknowledgements

We are grateful to Prof. R. C. Budhani, Director, National Physical Laboratory, New Delhi, India for providing the facilities. S.K. Mishra is thankful to the Council of Scientific and Industrial Research, India for providing a senior research fellowship (SRF).

[a] *CSIR-National Physical Laboratory, Dr. K.S. Krishnan Road, New Delhi-110012, India*

E-mail: rajesh_csir@yahoo.com
[b] *Department of Applied Chemistry, Delhi Technological University, Bawana Road, Delhi-110042, India*

References

1. G. Hodes, *Adv. Mater.* **,**2007, **19**, 639.
2. M. Adaris, L. Marzo, J. Pons, D. A. Blake and A. Merkoçi, *Biosens. Bioelectron.* ,2013**, 47**, 190.
3. W. Wu, M. Wu, Z. Sun, G. Li, Y. Ma, X. Liu, X. Wang and X. Chen, *J. Alloys Compd.,* 2013**, 579**, 117.
4. Y. Chen, Y. Tang, S. Luo, C. Liu and Y. Li , *J. Alloys Compd.* ,2013**, 578**, 242 .
5. X. Xu, X. Liu, Y. Li and Y. Ying, *Biosens. Bioelectron.,* 2013, **47**, 361.
6. Q. Kang, L. Yang and Q. Cai, *Bioelectrochemistry,* 2008, **74**, 62.
7. J. Wang, D. F. Thomas and A. Chen, *Anal. Chem.,* 2008, **80**, 997.
8. S. J. Kwon and A. J. Bard, *J. Am. Chem. Soc.,* 2012, **134**, 10777.
9. T. Kong, R. Su, B. Zhang, Q. Zhang and G. Cheng, *Biosens. Bioelectron.* ,2012, **34**, 267.
10. A. Qureshi, Y. Gurbuz and J. H. Niazi, *Sens. Actuators, B,* 2012, **171**, 62.
11. B. McDonnel, S. Hearty, P. Leonard and R. O'Kennedy, *Clin. Biochem.* ,2009, **42**, 549.
12. N.S.K. Gunda and S.K. Mitra, *Biomicrofluidics,* 2010**,4**, 014105.
13. J.F. Masson, L. Obando, S. Beaudoin and K. Booksh, *Talanta,* 2004, **62**, 865.
14. F. Darain, P. Yager, K. L. Gan and S. C. Tjin, *Biosens. Bioelectron.,* 2009, **24**, 1744.
15. E. G. Matveeva, Z. Gryczynski and J. R. Lakowicz, *J Immunol Methods* ,2005, **302**, 26.
16. L. Bonel, J. C. Vidal, P. Duato and J. R. Castillo, *Anal. Methods* ,2010,**2**, 335.
17. B. Jeong, R. Akter, O. H. Han, C. K. Rhee and M. A. Rahman, *Anal. Chem.* ,2013, **85**, 1784.
18. Li, L.T. Xiao, G.M. Zeng, G.H. Huang, G.L. Shen and R.Q. Yu, *J. Agric. Food Chem.* ,2005, **53**, 1348.
19. S. K. Arya, T. S. Pui, C. C. Wong, S. Kumar and A. R. A. Rahman, *Langmuir* ,2013, **29**, 6770.
20. Q. Wei, Y. Zhao, B. Du, D. Wu, H. Li and M. Yang, *Food Chemistry,* 2012**, 134**,1601.
21. S. Pakapongpan, R. Palangsuntikul and W.Surareungchai *Electrochim. Acta* ,2011, **56**, 683.
22. A. Venkatanarayanan, T.E. Keyes and R.J. Forster, *Anal. Chem.*, 2013, **85**, 2216.
23. S. Shrikrishnan, K. Sankaran and V. Lakshminarayanan, *J. Phys. Chem. C*, 2012, **116**, 16030.
24. Y. Teow and S. Valiyaveettil, *Nanoscale* ,2010, **2**, 2607.
25. E. T. Vandenberg, L. Bertilsson, B. Liedberg, K. Uvdal, R. Erlandsson, H. Elwing and I. Lundstrom, *J. Colloid Interface Sci.,* 1991, **147**,103.
26. A. Barth, *Biochim. Biophys. Acta*, 2007,**1767,**1073.
27. L. Yang and Y. Li, *Biosens. Bioelectron.* ,2005**,20**, 1407.
28. S.A. Mamuru and K.I. Ozoemena, *Electroanalysis* ,2010, **22**, 985.
29. V.Ganesh, S.K. Pal, S.Kumar and V. Lakshminarayanan, *J. Colloid Interface Sci.* ,2006, **296**,195.
30. E.V. Suprun, A. L. Shilovskaya, A.V. Lisitsa, T.V. Bulko, V.V. Shumyantseva and A.I. Archakov, *Electroanalysis* ,2011**, 23,** 1051.
31. S. K. Mishra, D. Kumar, A. M. Biradar and Rajesh, *Bioelectrochemistry* ,2012,**88** ,118.
32. Rajesh , V. Sharma, V.K. Tanwar, S.K. Mishra and A.M. Biradar , *Thin Solid Films* , 2010, **519**, 1167
33. S.S. Mandal, K. K. Narayan and A. J. Bhattacharyya, *J. Mater. Chem. B,* 2013, **1**, 3051
34. Y. Wang, Y. Zhou, J. Sokolov, B. Rigas, K. Levon and M. Rafailovich, *Biosens. Bioelectron.* ,2008, **24**, 162.
35. M. Billah, H. C. W. Hays and P. A. Millner, *Microchim. Acta,* 2008, **160**, 447.

